BER | the international journal of bridge engineering management and research

Innovative Repair of Transversely Cracked PPC Bridge Deck Girders Using Precast Prestressing Plates with Shape Memory Alloys

Dachina Gunasekaran; Arslan Qayyum Khan; and Bassem Andrawes*

Submitted: 22 May 2025 **Accepted:** 27 June 2025 **Publication date:** 10 July 2025

DOI: 10.70465/ber.v2i3.39

Abstract: The highway infrastructure in the United States is facing increasing performance and durability issues due to aging. One of the recent issues faced by precast prestressed concrete (PPC) deck girder bridges is the occurrence of transverse cracks in the soffit of the girders. Transverse cracks adversely affect the capacity and ductility of the girder and lead to increased stresses in the strands. There is an increasing need to repair and mitigate the effects of transverse cracks in these girders. This paper proposes an innovative repair of transversely cracked PPC bridge deck girders using shape memory alloy precast prestressing plates (SMA-PPP). The feasibility of applying external prestressing using voided SMA-PPPs was investigated experimentally by affixing them to a mortar block. The mortar block successfully developed the expected prestress and exhibited a 50% improvement in capacity compared to a control block under a four-point bending test. A numerical investigation was also conducted to assess the improvement in capacity and load rating of a transversely cracked PPC deck girder repaired using voided SMA-PPPs. Furthermore, a parametric study was conducted to assess the influence of the width of transverse cracks, the length of the PPP, and the SMA–concrete area ratio on the improvement in the capacity and load rating of the repaired girders. The numerical analysis demonstrated a 36% improvement in the capacity of the repaired girders, which resulted in a 40.91% improvement in the load rating.

Author keywords: Bridge girder; external prestressing; concrete repair; precast prestressing plate; shape memory alloys

Introduction

Prestressed concrete bridges account for nearly a third of all the bridges in the United States. Among the many types of prestressed bridges, precast prestressed concrete (PPC) deck girder bridges (also known as adjacent box girders) are a prevailing choice (one-third of all the prestressed concrete bridges), especially for short to medium-span bridges. According to the National Bridge Inventory,[1] nearly 5% of the PPC deck girder bridges in the United States are in "poor" condition, and an additional 6.7% of bridges are forecasted to deteriorate to poor condition in the next decade. Therefore, the PPC deck girder bridges are fading out of popularity due to durability and performance issues that arise due to the formation of longitudinal and transverse cracks and corrosion, which affect the capacity and performance of the bridges.

Transverse cracks, the most critical cracks, occur at the bottom (tension face) of the girder and cause a reduction in the capacity of the girder and a buildup of stresses in the girder, thereby affecting the capacity and serviceability of the girder. They could expose the strands to the environment, leading to corrosion and exacerbating the strength and durability issues. The effect of a transverse crack on a damaged girder's performance can be measured using the capacity and built-up stresses, which are used to load rate the girder. In Xiaohong,[2] a continuous prestressed box girder bridge adversely affected by transverse cracks was studied. It was observed that the transverse cracks caused increased deflection and higher tensile stresses at the soffit of the girders. This example highlights the adverse effects of transverse cracks on a bridge's structural safety and performance. In a recent study by Gunasekaran et al.,[3] an in-service 838 mm × 914 mm Illinois Department of Transportation PPC girder with a transverse crack was tested at the University of Illinois at Urbana-Champaign (UIUC). It was observed that the girder exhibited an elastic capacity 34% lower than its nominal capacity, and the strand stresses at the crack, predicted using analytical models, could be 29% higher than in the uncracked girder. Thus, the load rating of the girder was significantly impacted, and the girder was predicted to have a rating below zero, rendering the girder unusable. This shows the importance of assessing the residual capacity and the strand stresses at a transverse crack.

In permissible cases, retrofitting the damaged girder to ensure adequate strength and serviceability would be more

---

*Corresponding Author: Bassem Andrawes.
Email: andrawes@illinois.edu
Department of Civil and Environmental Engineering, University of Illinois at Urbana-Champaign, Urbana, IL 61801, USA

Discussion period open till six months from the publication date. Please submit separate discussion for each individual paper. This paper is a part of the Vol. 2 of the International Journal of Bridge Engineering, Management and Research (© BER), ISSN 3065-0569.

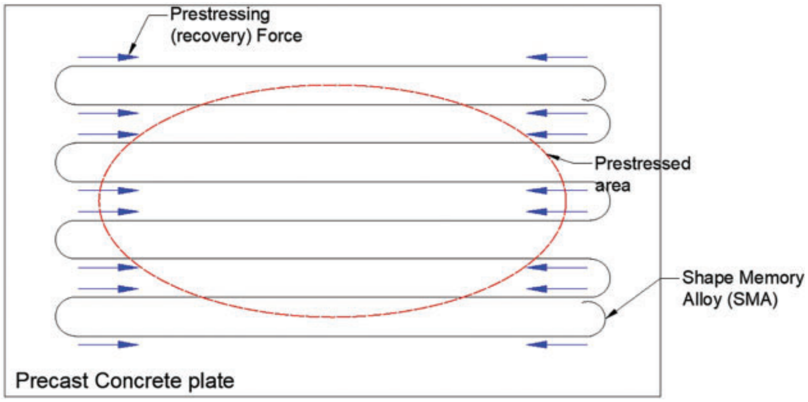

Figure 1. Plan view of an SMA-PPP showing the flow of prestressing forces across the specimen

economical and eco-friendly than constructing a new bridge. The external retrofitting methods adopted can be prestressed or non-prestressed in nature. External prestressing is a method where the prestressing strands/tendons are located outside the concrete section. Since the 1990s, it has been extensively used to retrofit and rehabilitate prestressed concrete structures. External prestressing has also been used to control deflections and to increase the sectional capacity Xiaohong.[2,4] The drawbacks associated with the traditional external prestressing method include (i) expensive equipment to prestress and anchor the strands, (ii) the requirement of sufficient space for bulky steering blocks, instruments, and anchorage systems, (iii) the need for routine maintenance, which could increase the associated cost of the bridge,[5–7] and (iv) external prestressing tendons are also prone to corrosion.[8]

In the past three decades, shape memory alloys (SMAs) have been used to provide innovative structural engineering solutions like seismic isolators, energy-dissipating braces, dampers,[9,10] prestressing elements, and in repairing and strengthening steel and concrete structures in flexure and shear.[6,11–13] SMAs are metals that can return to their original shape when heated, a behavior known as the shape memory effect (SME). This occurs through a microstructural phase transformation from martensite to austenite upon heating above the austenite finish temperature (A_f). If the SMA is restrained during this transformation, it generates a recovery stress, which can be harnessed to apply prestress in civil engineering applications.[6,11,13] In an experimental study by Zhao and Andrawes,[6] an innovative prestressing method using an SMA precast prestressing plate (SMA-PPP) was introduced. As the SMA wires were bent at the ends (see Fig. 1), they were self-anchored to the precast plate and restrained against moving or slipping. Upon heating and cooling, the SMA wires developed their recovery stress and, in turn, prestressed the mortar enclosed between the ends of the wire. Thus, the PPP developed a prestressed area in the middle, as shown by the area in the red ellipse in Fig. 1. This is the mechanism by which the concrete plate is prestressed using SMA. When voids were introduced in the plate, there was a notable reduction in the self-weight of the repair mechanism, thereby inducing higher stress in the plate and repaired member for the same prestressing force. There was also a decrease in the tensile demand on the adhesive layer due to the reduced plate weight. When the SMA bars were placed in the voids, it allowed for faster heating and cooling of the bars compared to when they were encased in concrete.

In previous studies,[6,13–15] smaller-diameter wires (1–2 mm) were used, as they were commercially available in a heat-treated and prestrained state, ready for use in prestressing applications. However, for real-world practical applications, larger-sized SMA wires and bars are needed. Due to the different treatment and working that the material undergoes at various sizes, the behavior of the large-sized SMA wires is expected to be different from that of smaller-sized wires. Thus, this study investigates the use of larger-sized (6.3 mm diameter) NiTiNb bars with a recovery stress of 275 MPa. From the literature review, it was found that there is a need to experimentally investigate the prestressing capabilities of the 6.3-mm SMA bars and the improvement in the flexural capacity of concrete members when repaired using SMA-PPPs. There is also a need to examine the feasibility of repairing large-scale damaged girders using SMA-PPPs numerically. This study addresses these needs by (i) developing the concept of voided SMA-PPPs, (ii) experimentally investigating the prestressing effect of voided SMA-PPPs with the 6.3-mm NiTiNb bars, (iii) developing and experimentally validating a numerical model of the voided SMA-PPPs, and (iv) extending the concept of repair using voided SMA-PPPs to girders damaged by transverse cracks.

Proof-of-Concept Voided SMA-PPP

Description of test specimens

In this study, two PPPs were fabricated, one without SMA bars and the other reinforced with SMA bars. The PPP specimen dimensions were 304 mm × 152 mm × 19 mm, as illustrated in Fig. 2a. Both PPP specimens had two rectangular voids in the middle, with dimensions of 184 mm × 44 mm, positioned along the long direction and at the center of the plate. These voids primarily optimized the use of materials by

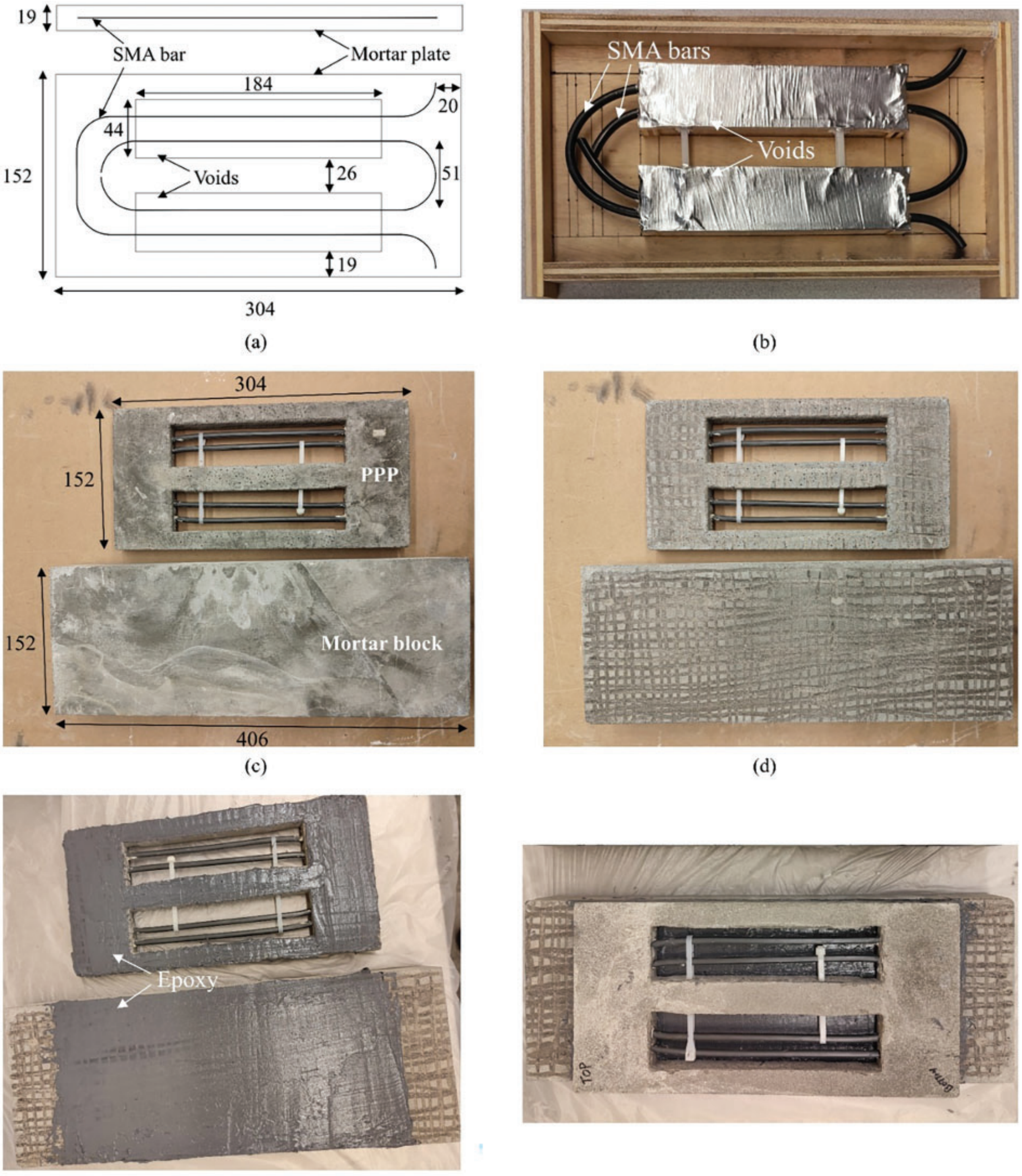

(a) (b) (c) (d) (e) (f)

Figure 2. Details of specimen: (a) schematic of PPP (units in mm); (b) mold of PPP with SMA bars; (c) PPP and block after demolding; (d) surface preparation; (e) epoxy application; and (f) PPP attached to block

reducing the amount of mortar required. Furthermore, these voids facilitated the effective heating of the embedded SMA bars by allowing the bars to be exposed in the void region.

The SMA-PPP included two SMA bars shaped to provide efficient prestressing and self-anchorage. Each SMA bar was bent 180° at one end, forming two legs. The opposite ends of the outer SMA bar were bent 90° to secure the bars inside the PPP, creating four legs. The straight sections of the SMA legs passed through the voids in the PPP, allowing the open ends of the bars to be used for heating by passing an electric current. The NiTiNb SMA bars with a diameter of 6.3 mm were used. According to the energy-dispersive X-ray spectroscopy analysis results, the chemical composition comprised 55% Ni, 36% Ti, and 13% Nb by weight.[16] This alloy was chosen for its wide thermal hysteresis and relatively high recovery stress. The elastic modulus of the bars used is 87,870 MPa, and the yield stress is 500 MPa. With a thermal hysteresis range exceeding 200°C, NiTiNb SMA could maintain a recovery stress of approximately 275 MPa at ambient temperature.[17] These already prestrained SMA bars were bent into shape and placed at the mid-height of the PPP specimen before casting the mortar. A schematic diagram showing the PPP, voids, SMA legs, and dimensions is presented in Fig. 2a.

The formwork used to cast the PPP was made from wood, and the voids were covered with aluminum foil to prevent mortar from entering the voids during the casting process, as shown in Fig. 2b. In addition to the PPP specimens, two mortar blocks with dimensions of 406 mm × 152 mm × 51 mm were cast concurrently with the PPP to ensure consistency in mortar strength between the PPP specimens and the mortar blocks. Furthermore, six mortar cylinders with dimensions of 102 mm in diameter and 203 mm in height were also cast to determine the compressive strength of the mortar. The specimens were demolded 24 hours after casting and cured for 28 days, as shown in Fig. 2c. After demolding, the surfaces of the PPP and the mortar block were prepared for bonding by sanding and creating grooves with a grinder to ensure good adhesion between the epoxy and the mortar. This surface preparation step, illustrated in Fig. 2d, was crucial for creating a strong bond between the PPP and the block. Following the surface treatment, epoxy was applied uniformly to both the PPP and the mortar block, as shown in Fig. 2e. After ensuring a consistent thickness of epoxy, the PPP was carefully attached to the block, and steel weights were placed on top of the PPP to maintain firm contact and ensure proper bonding. The assembly was left to cure for 48 hours. After curing, the weights were removed, and the PPP was found to be perfectly bonded to the block, as shown in Fig. 2f.

Experimental test setup and results

The test setup for the SMA-PPP attached to the mortar block is shown in Fig. 3a. The specimen was placed on two circular steel rods serving as vertical supports. Two strain gauges were strategically installed to monitor the strain response during the activation of the SMA bars. The first strain gauge (S1) was attached just above the bonding interface in the center of the PPP. Another strain gauge (S2) was placed right underneath the interface in the center of the block. This strain gauge setup was established to measure the transfer of prestressing force from the PPP to the block through the bonding interface. The strain measurements of both the PPP and the block were used to monitor the prestressing effect induced by the SMA activation and to assess the effectiveness of the bond between the two components.

The SMA bars in the PPP consisted of four legs, which passed through the rectangular voids in the PPP. The exposed ends of the SMA bars were connected to a potentiostat using copper wires and electrical clamps to produce the electrical current necessary to heat the bars, as shown in Fig. 3a. The heating of the SMA bars triggered the SME, allowing the bars to introduce compressive forces into the PPP. A thermocouple was attached to the middle of the exposed SMA leg to monitor the temperature of the SMA bars and avoid overheating. The target activation temperature was 200°C, ensuring the complete activation of the NiTiNb SMA bars while preventing overheating.

Each SMA leg was heated one at a time to the target temperature, and once the temperature reached 200°C, the electrical power was shut off. This sequential heating of the four SMA legs ensured uniform activation of the prestressing force. After heating all four SMA legs, the specimen was allowed to cool to room temperature. Throughout the heating and cooling process, strain data were continuously recorded by a data acquisition system to capture the real-time response of both the PPP and the block.

The compressive strength of the mortar used in the experiment, determined from the cylinder tests, was 64 MPa on the day of testing. The strain response over time for both strain gauges (S1 and S2) is shown in Fig. 3b. During the heating phase, strain oscillations were observed in the data, which can be attributed to the sequential heating of the SMA legs and the resulting shape recovery process. At the end of the cooling phase, the strain in the PPP (S1) reached a stable value of $-83\ \mu\varepsilon$, while the strain in the mortar block (S2) stabilized at $-53\ \mu\varepsilon$, both in compression. The stable compressive strains indicated that the SMA bars generated recovery stress, which was effectively transferred across the interface. Based on the stress–strain relationship obtained

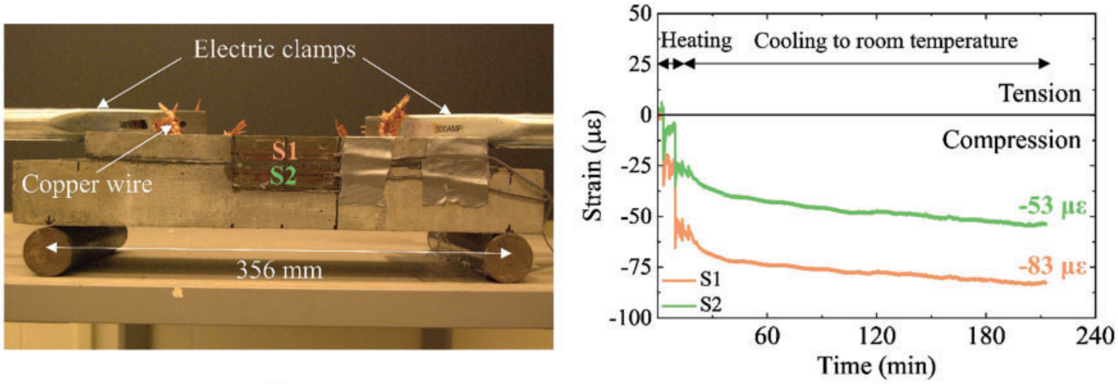

(a) (b)

Figure 3. SMA activation: (a) test setup and (b) strain gages' readings

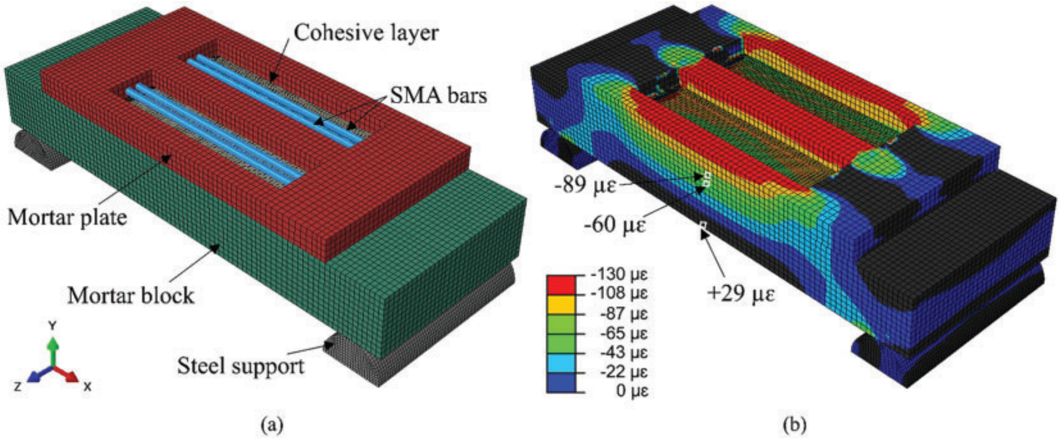

Figure 4. Numerical analysis: (a) assembly of the model and (b) strain distribution

from the mortar cylinder tests, the corresponding compressive stress in the PPP when the strain reached -83 με was approximately 3.12 MPa. Similarly, the compressive stress in the mortar block, associated with a strain of −53 με, was approximately 2.0 MPa. These results validated that the SMA activation produced significant compressive stresses in the PPP and that these stresses were successfully transferred to the mortar block.

Numerical analysis of SMA-PPP

A three-dimensional (3D) numerical model of the SMA-PPP attached to the mortar block was developed using the finite element (FE) software ABAQUS[18] to validate the experimental results. The assembly of the model is illustrated in Fig. 4a. The mortar plate, block, and steel supports were modeled using C3D8 elements. The SMA bar, which had the same geometry and bending configuration as the experimental specimen, was modeled using B31 beam elements. To ensure full anchorage between the SMA bars and the surrounding mortar, the embedded region feature was employed for the bent sections of the SMA bars inside the mortar plate.

A concrete damage plasticity model was utilized for the mortar, with a Young's modulus (E_c) of 37.6 GPa and a Poisson's ratio of 0.2. The concrete damage plasticity model required several additional parameters to describe the material's plastic behavior, including a dilation angle of 30°, an eccentricity of 0.1, a ratio of initial biaxial to uniaxial compressive strength (f_{b0}/f_{c0}) of 1.16, a K value of 0.6667, and a viscosity parameter of 0. These values were chosen based on material characterization and previous research.[6] To prestress the SMA bars, a temperature field combined with a negative thermal expansion coefficient was applied to the straight sections of the SMA bars passing through the voids, ensuring that the recovery stress in the SMA bars reached the desired value of 275 MPa.

To simulate the bonding, the epoxy adhesive between the PPP and the mortar block was modeled as a 2-mm thin cohesive layer tied to both surfaces. The behavior of the epoxy at the interface was captured using a traction-separation law in ABAQUS.[18] Three parameters were defined to represent the adhesive's behavior: the normal modulus (E_{nn}) and the shear moduli (E_{ss} and E_{tt}). Based on Zhao and Andrawes,[6] the moduli (E_{nn}, E_{ss}, and E_{tt}) and maximum shear stress in the model were set to 34.5 MPa and 7.9 MPa, respectively. For normal separation, the maximum stress was equal to the tensile strength of the concrete, representing bond failure at that limit.

The strain distributions obtained from the numerical analysis are shown in Fig. 4b. The model indicated compressive strain within the prestressed area of the plate, while tension was visible at the bottom of the mortar block. The strain distributions showed that the prestressing forces in the PPP were efficiently transferred to the mortar block through the epoxy layer. No signs of debonding at the interface were observed. This observation confirmed the adequacy of the epoxy in maintaining a strong bond between the plate and the block. Furthermore, the tensile strain observed at the bottom of the block proved that the activated SMA bars produced substantial compressive stress in the PPP, which was successfully transferred to the mortar block.

A comparison of the strain values from the numerical model with the experimental results was performed to validate the numerical analysis. The strain measured in the PPP (S1) from the numerical model was found to be −89 με, which was only 7% higher than the experimental value of −83 με. Furthermore, the strain in the mortar block (S2) was −60 με, with a 13% difference from the experimental value of −53 με. These relatively small differences between the numerical and experimental strain values indicated a satisfactory agreement, suggesting that the numerical model accurately replicated the experimental behavior.

This validation is crucial for ensuring the accuracy and reliability of the beam analysis in the subsequent sections. By closely replicating the experimental strain values, the numerical model lays a solid foundation for predicting the prestressing effects and performance improvements of the SMA-PPP in full-scale beam applications.

Flexural test setup and results

A four-point bending test was conducted on the two specimens to assess the flexural performance of the PPP bonded to a mortar block. The first specimen consisted of a PPP

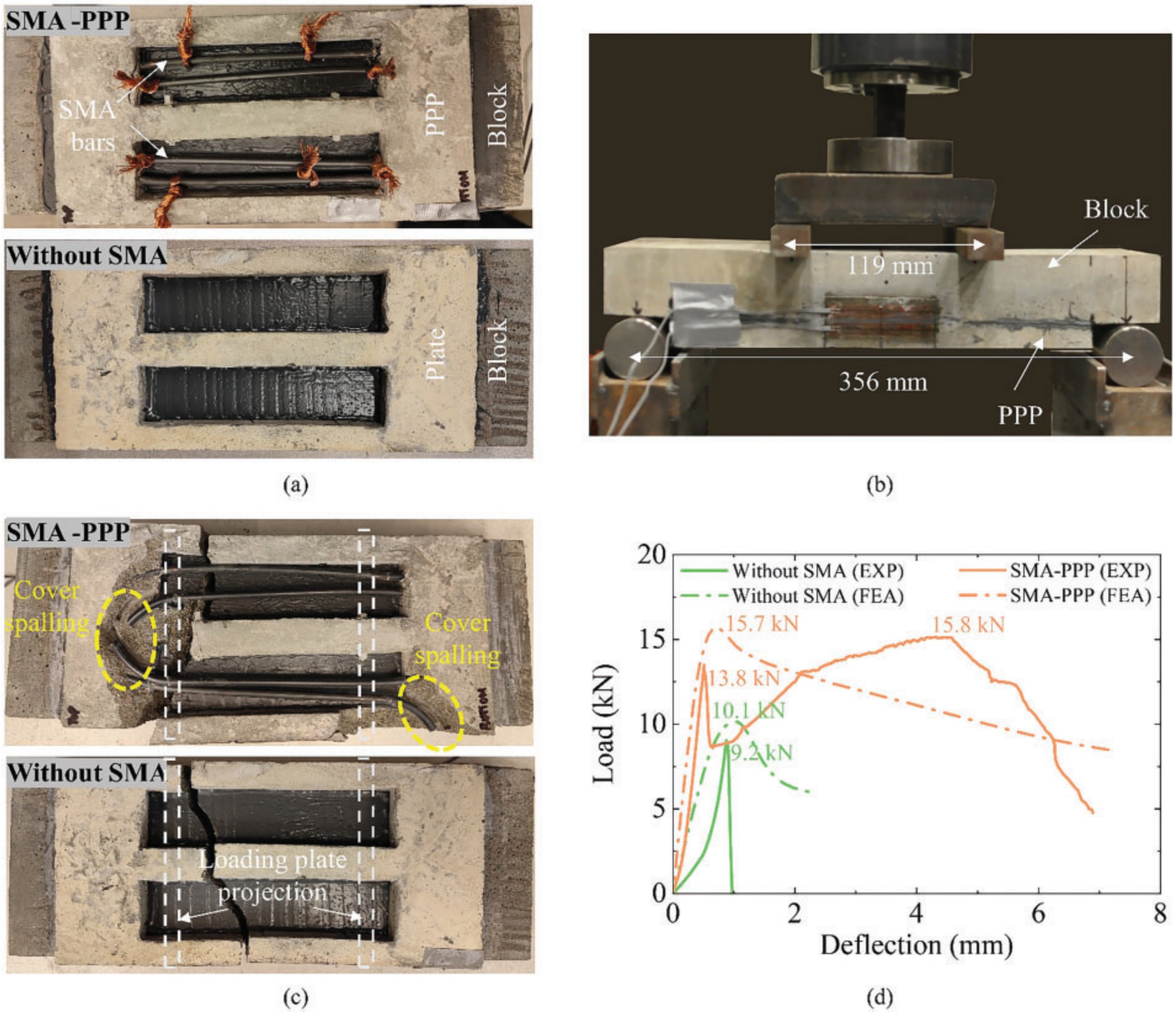

Figure 5. Flexural test setup and results: (a) specimens; (b) test setup; (c) failure mode; and (d) load–deflection curves comparison

reinforced with SMA bars bonded to a mortar block, and the second was a plate without SMA. These two specimens are shown in Fig. 5a. The specimens were inverted in the flexural test setup. Subsequently, the mortar block was placed on top, and the PPP was placed on the lower side, as shown in Fig. 5b. The specified setup was employed to replicate real-world conditions, where the PPP would be positioned on the tension side of a structural member. The test was conducted using a 110 kN universal testing machine (UTM) in displacement control mode. The load was applied at a displacement rate of 1 mm/min. The four-point bending test was preferred as it eliminates the shear stresses in the bending region, enabling accurate assessment of the flexural behavior of the specimens. The supports were placed 356 mm apart, while the distance between the loading plates was taken as one-third of the effective span, which was 119 mm. This arrangement ensured that the mid-section of the specimen experienced pure bending under the applied load.

The failure modes of the two specimens were distinct and provided insight into the role of SMA reinforcement in improving the flexural capacity of the PPP. The failure progression for both specimens is illustrated in Fig. 5c. The specimen with SMA bars embedded in the PPP exhibited a ductile failure mode. The initial crack formed at the bottom of the PPP, where the tensile stresses were the highest. Then, the crack extended vertically with the increase in load. Once the crack was initiated, the SMA bars took over the load-carrying responsibility. The load was progressively transferred from the cracked concrete to the SMA bars, which provided additional capacity and delayed failure. With further loading, localized spalling of the concrete cover around the bent SMA bars was observed, but the specimen continued to sustain load without sudden failure. This behavior demonstrated the capacity of the SMA bars to carry tensile forces after cracking, contributing to the ductility of the system. The specimen exhibited visible warning signs of failure, such as spalling, the metallic sound of SMA, and large deflections, revealing its ductile behavior. On the other hand, the specimen without SMA bars failed in a brittle manner. The specimen exhibited an abrupt failure with a sudden drop in load-carrying capacity upon cracking. The initial crack also formed at the bottom of the PPP, but in the absence of SMA reinforcement, there was no mechanism to continue carrying the load after the crack formed. Consequently, the specimen failed quickly after the first crack appeared, showing minimal deformation or warning before failure.

The load–deflection curves of both specimens are shown in Fig. 5d. The specimen with SMA bars had its first crack at 13.8 kN. After cracking, load redistribution allowed it to recover and resist up to 15.8 kN. The specimen displayed gradual, ductile failure with a stiffness of 18 kN/mm, providing critical warning signs before failure. In contrast, the specimen without SMA bars cracked at 9.2 kN, 50% lower than the specimen with SMA bars. It failed abruptly with limited deformation, showing a maximum stiffness of 10 kN/mm and no post-cracking load capacity.

Furthermore, to validate the developed FE model, numerical load–deflection curves were obtained using ABAQUS[18] and are also shown in Fig. 5d. Overall, the model demonstrated good agreement with the experimental results. For the SMA-PPP specimen, the peak load was predicted at 15.7 kN, which is within 0.6% of the experimentally observed peak of 15.8 kN. For the control specimen without SMA, the model predicted first cracking at 10.1 kN, compared to 9.2 kN in the experiment, representing a 9.8% deviation, which is acceptable given material and boundary variability. It is worth noting that the experimental curves showed softening at the early loading stage, which is likely due to machine compliance and system deformation in the UTM. To eliminate the effects of this initial softening, stiffness values were calculated beyond the softening region in the experimental curves. For the SMA-PPP specimen, the initial stiffness was found to be 33.04 kN/mm experimentally and 33.28 kN/mm from the numerical model, reflecting a very small difference of 0.7%. For the control specimen without SMA, the experimental stiffness was 15.28 kN/mm, while the model predicted 14.68 kN/mm, resulting in a 3.9% difference. These results confirm that the developed model accurately captures the initial stiffness and peak load of both specimens. However, some deviations in the post-cracking region were observed, particularly for the SMA-PPP specimen, where the numerical response was more idealized compared to the gradual softening after cracking seen in the experiment. These differences are attributed to local imperfections, variability in bonding and cracking behavior, and idealizations in the numerical model, such as perfect bonding assumptions and homogenized material properties.

In summary, the inclusion of SMA bars in the PPP design significantly enhanced the flexural capacity of the system, providing both increased strength and ductility. The concept of voided SMA-PPPs as a repair measure for transversely cracked PPC deck girders was numerically assessed and the results and observations are presented in the next section. The damaged PPC deck girder exhibited reduced capacity, ductility, higher built-up stresses, and an early onset of nonlinear behavior compared to the uncracked girder.[3] The damaged girder that was experimentally tested in Gunasekaran et al.[3] was repaired with voided SMA-PPPs and the improvement in capacity, ductility, and load rating of the girder were numerically assessed and presented in the next section. The impact of the variations in the PPP length, transverse crack width, and the SMA–concrete area ratio were also considered.

Numerical Analysis of Repaired Girders

Fig. 6a shows the cross-section of the 838 mm × 914 mm PPC deck girder considered in this study. The girder was extracted from the approach span of a three-span simply supported bridge in Schuyler County, Illinois. It was constructed in 1984 according to AASHTO LFD specifications and was in service for 38 years. It was found to have a transverse crack (Fig. 6b) at the bottom of the girder, located near the midspan, adjacent to the middle diaphragm of the girder.

The girder was 14.1 m long, with a 10° skew. As shown in Figure 6a, the girder had seven 12.5 mm G270 low-relaxation prestressing strands with an ultimate strength of 1862 MPa. The strands were located 44.5 mm from the bottom of the girder and had an eccentricity of 372.1 mm. The

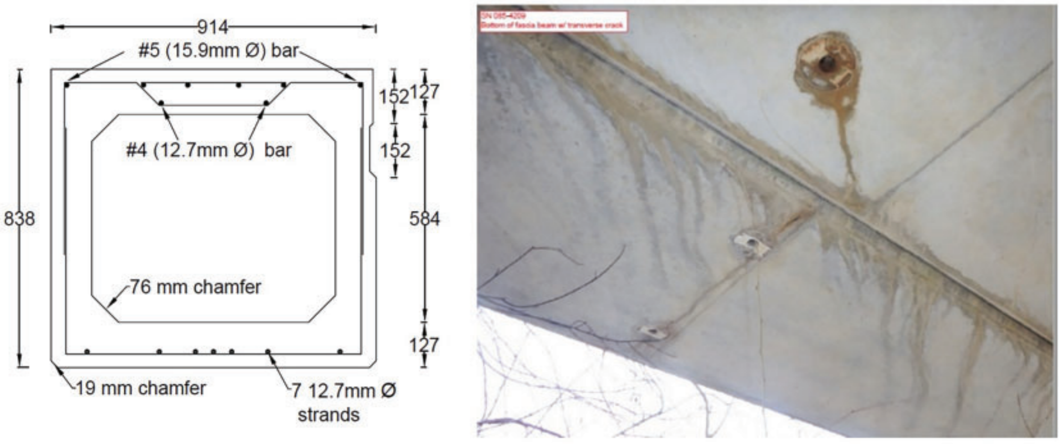

(a) (b)

Figure 6. Details of PPC deck girder: (a) schematic cross-section and (b) location of the transverse crack on girder

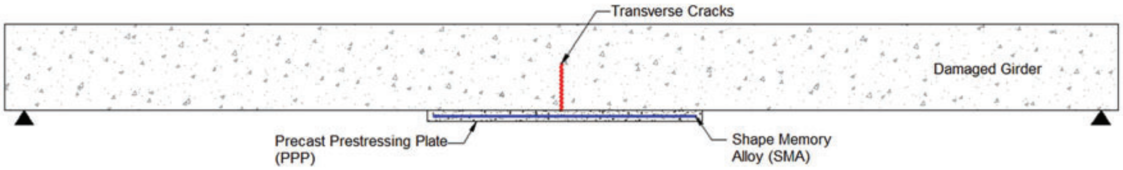

Figure 7. Schematic sketch of damaged girder repaired with SMA-PPP

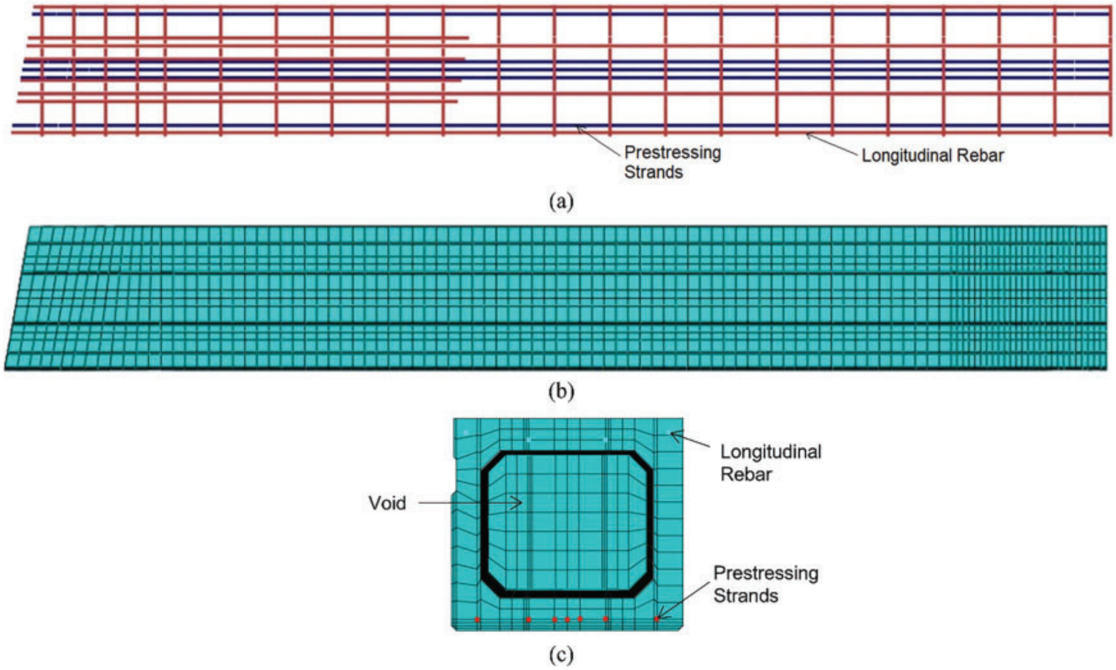

Figure 8. A rendered view illustrates the partial plan view of (a) the internal reinforcements; (b) the concrete girder; and (c) the cross-sectional view of the girder in ABAQUS

girder was specified to have a concrete strength of 34.5 MPa at 28 days. The girder had 838-mm-wide diaphragms at the ends and a 467-mm-wide diaphragm at its midspan.

The girder was extracted and tested at the Newmark Structural Engineering Laboratory at the UIUC. Upon visual inspection of the damaged girder, eight cracks were identified and marked on the girder. The transverse crack near the middle was caused by the flexural response of the girder, while the other cracks were due to the shear-torsional response. The details of the experimental and numerical study of the damaged girder were published in Gunasekaran et al.[3]

In this study, a numerical simulation of the cracked and then repaired 838 mm × 914 mm PPC deck girder specimen was conducted using ABAQUS. The simulation was conducted to assess the effectiveness of using the SMA-PPP repair technique to improve the capacity and load rating of cracked girders. In the FE analysis, the girder was initially loaded to induce transverse cracks of varying crack widths and then unloaded. It was then repaired with the SMA-PPP (Fig. 7) and loaded under the design live load as per AASHTO LRFD (HS-20 wheel loads). The behavior under the live load was studied to understand the effect of using SMA-PPP. The study investigated the improvement in the load rating of the repaired girder due to variations in three parameters: the width of the transverse crack, the length of the PPP, and the amount of SMA in the cross-section.

FE model description

The PPC deck girder was modeled as a simply supported girder with pinned and roller supports on either end. The supports were placed at a center-to-center distance of 13.34 m and a skew of 10° to emulate the support conditions of the bridge when it was in service. Three loading plates were placed 4.27 m apart to simulate a single-wheel line of the HS-20 truckload. The concrete girder and the internal reinforcement, including the prestressing strands, longitudinal rebars, and stirrups, were modeled using the material properties and dimensions in the bridge plan. Figs. 8a, 8b shows the rendered plan view of the internal reinforcements and the concrete girder, and Fig. 8c shows the cross-section of the girder.

In ABAQUS, the concrete damage plasticity model was used to model the concrete material properties, while a plasticity model was used to model the prestressing strand and rebar material properties.[18] The stress–strain behavior of the prestressing strands and the concrete elements was modeled using the Menegotto–Pinto[19] and Hognestad[20]

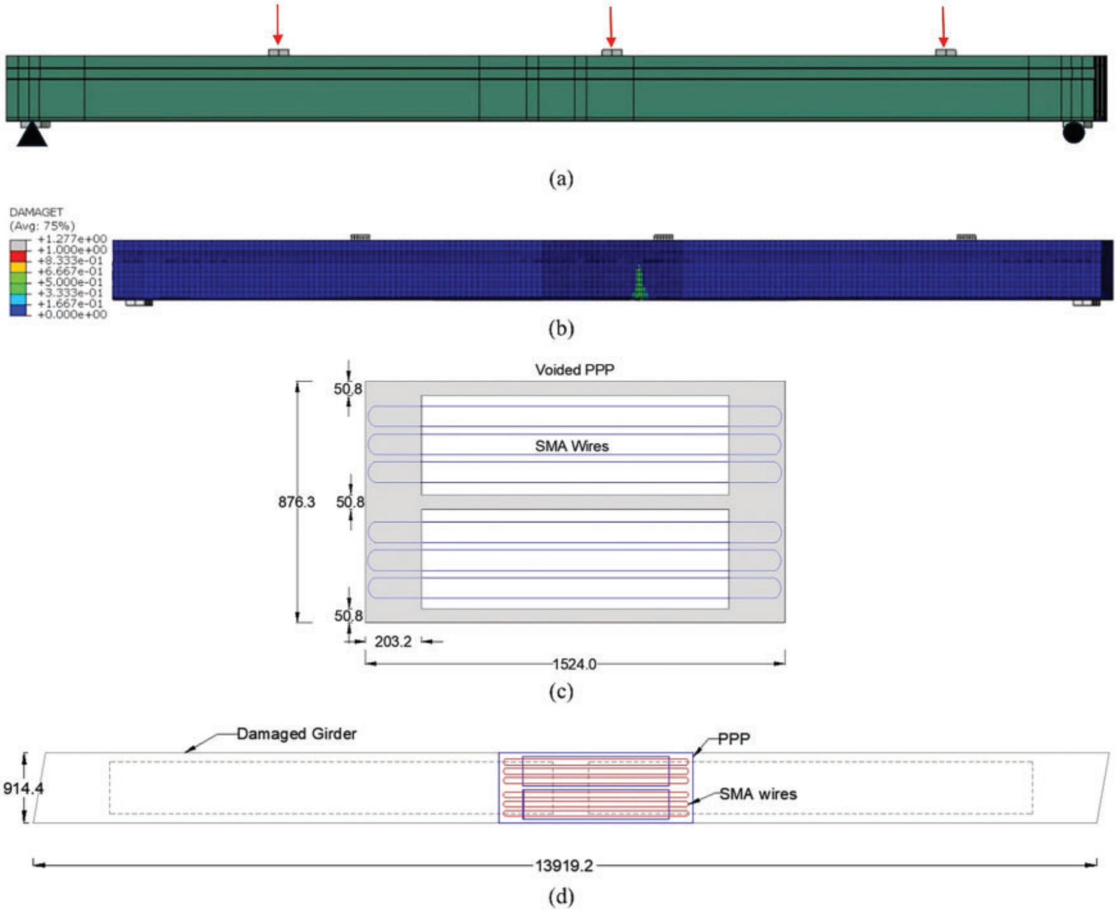

Figure 9. (a) Elevation view of the HS-20 wheel loads on the prestressed girder; (b) damage contour illustrating the transverse crack in the elevation view of the girder; (c) sketch of the plan view of a 1.52-m-long SMA-PPP; and (d) damaged girder repaired with SMA-PPP (units in mm)

models, respectively. A bilinear elastoplastic model was used to model the stress–strain behavior of the internal rebars.

The longitudinal and transverse rebars were embedded in concrete, assuming a perfect bond. Nonlinear spring elements were used to model the bond-slip behavior between the prestressing strands and the concrete elements. An average bond stress of 7.1 MPa was used for the 12.7 mm G270 prestressing in the analysis. The average bond stress was obtained by multiplying a factor of 4.0 ($\sim$1.9 × 2.1) by the average pullout bond stress from the literature.[21–25] The modification factor of 4 accounts for the difference between the maximum and average (2.1) pullout bond strength[25] and the difference between tensioned and untensioned (1.9) pullout tests.[26] The bond-slip model used in this study is described in detail in.[27]

Loading setup

Fig. 9a shows the setup of the HS-20 wheel load that was applied to the prestressed girder to introduce a transverse crack near the mid-span of the girder. As shown in Fig. 9b, the transverse crack induced in the girder was tracked using the tension damage (DamageT) contours in the ABAQUS model. In the numerical study, three cracks with increasing levels of damage were considered: a hairline crack with a width of 0.13 mm, a moderate crack that could be easily observed by visual inspection with a width of 0.25 mm, and a severe crack with a width of 0.36 mm. These crack widths were chosen to observe the effectiveness of the repair method for the range of crack widths that could be observed in the field.

Once cracked, the HS-20 wheel loads were removed. An SMA-PPP (Fig. 9c) was attached to the girder (Fig. 9d) using a cohesive interface to simulate the epoxy layer. The SMA was then activated to prestress the PPP. The component stresses were then noted, and the repaired girder was loaded with an HS-20 wheel load to observe the improvement in the load-carrying capacity of the girders.

Modeling SMA-PPP: components and interface

The PPPs used to retrofit the damaged girders were rectangular plates made of 34.5 MPa concrete with two rectangular voids, similar to the PPP in Fig. 2a. The 6.3-mm SMA bars were used to prestress the plate. In the numerical analysis, three variations in the PPP length and SMA–concrete area ratios were considered. The lengths of the SMA-PPP considered in the analysis were 1.52, 3.05, and 4.57 m, and each SMA-PPP was modeled with six, twelve, and twenty-four SMA bars, resulting in SMA–concrete area ratios of

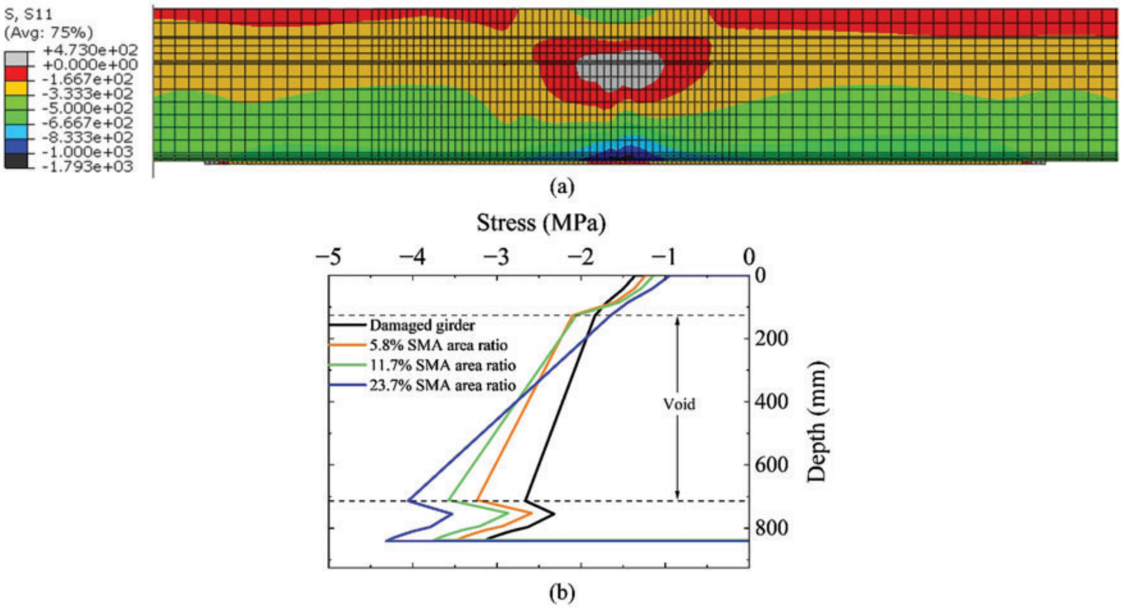

Figure 10. (a) Stress contour of the PPC deck girder repaired using a 4.57 m 23.4% SMA-PPP and (b) variation in stress distribution along the girder depth due to different SMA area ratios

3.9%, 11.7%, and 23.4%, respectively. A total of nine SMA-PPP configurations were analyzed for each of the three transverse crack widths (0.13, 0.25, and 0.36 mm). Fig. 9c shows the schematic plan view of a 1.52-m SMA-PPP with twelve 6.3-mm SMA bars (six bars in each of the two voids). As described in Section 3.3, the PPP and SMA bars were modeled as 3D solid C3D8 and B31 elements, respectively.

Results of the FE analysis

Fig. 10a presents the stress contour of the cracked PPC deck girder repaired using a 4.57-m-long SMA-PPP with a 23.4% SMA area ratio. The stress contour plot shows the additional compressive stress introduced in the girder due to the voided SMA-PPP. The 23.4% SMA-PPP introduced an additional 1.15 MPa of stress in the bottom of the girder. This is 44.9% of the stress in the PPC deck girder under the combined effect of self-weight and prestress.

Fig. 10b shows the stress distribution along the depth of the damaged and repaired girders. The section across the rectangular void in the girder was chosen to illustrate the effect of the SMA-PPP on the girder stresses. The stress induced due to the external prestress from the SMA-PPP showed a linear increase with increasing SMA–concrete area ratios. The stress at the top of the girder was reduced, and the compressive stress at the bottom increased with the application of external prestress from the SMA-PPP. The reduction in stress in the middle of the bottom flange is due to the presence of the crack.

Fig. 11a shows the load–displacement behavior of the damaged girder and the girder repaired using a 4.57–m-long 23.4% SMA-PPP. The elastic limit of the damaged and repaired girders was identified as the residual capacity to ensure elastic behavior under service loads.[3] The repaired girder showed a delayed onset of nonlinear behavior due to the additional capacity provided by the prestressing effect from the SMA-PPP. The elastic capacity and elastic displacement of the repaired girder exhibited notable improvements of 36.1% and 34.8%, respectively, compared to the damaged girder. The cohesive layer between the PPP and the girder showed no damage, even after the repaired girder exceeded its elastic capacity and exhibited nonlinear behavior. The two dashed lines represent the load demand due to the HS-20 wheel loads, with and without the distribution factor (DF) and with the impact factor (IM) for dynamic allowance. It is notable that the performance of the repaired girder remained elastic for the applied HS-20 wheel load, both with (HS20 × IM × DF) and without (HS20 × IM) the DF.

Figs. 11b–11d show the improvement in the elastic capacities of the girders repaired using a 1.52-, 3.05-, and 4.57-m-long SMA-PPP under the HS-20 wheel load. There was a linear increase in the elastic capacity as the area ratio of SMA increased from 5.8% to 23.4%. In Fig. 11b, there was a 16 kN (7.5%) and 62.5 kN (29.1%) improvement in elastic capacity for the girders repaired with 5.8% and 23.4% SMA-PPP, respectively. The increase in elastic capacity was attributed to the increased prestressing force in the higher SMA–concrete area ratios. The linear increase in elastic capacity was observed for all PPP lengths and crack widths. The increase in the SMA area ratio led to a linear reduction in the strand stresses (up to 0.65% reduction for the 23.4% SMA–concrete area ratio). The strand live load stresses under the HS-20 wheel load were also found to decrease linearly with increasing amounts of SMA, as the SMA carried part of the HS-20 wheel loads.

As the length of the PPP also increased, the area influenced by the prestressing effect of the SMA-PPP increased. In Fig. 11c, the elastic capacity of the girder repaired using a 23.4% area ratio SMA-PPP increased by 44.8 kN (21.2%), 60.9 kN (28.8%), and 64.1 kN (30.3%) for the 1.52-, 3.05-,

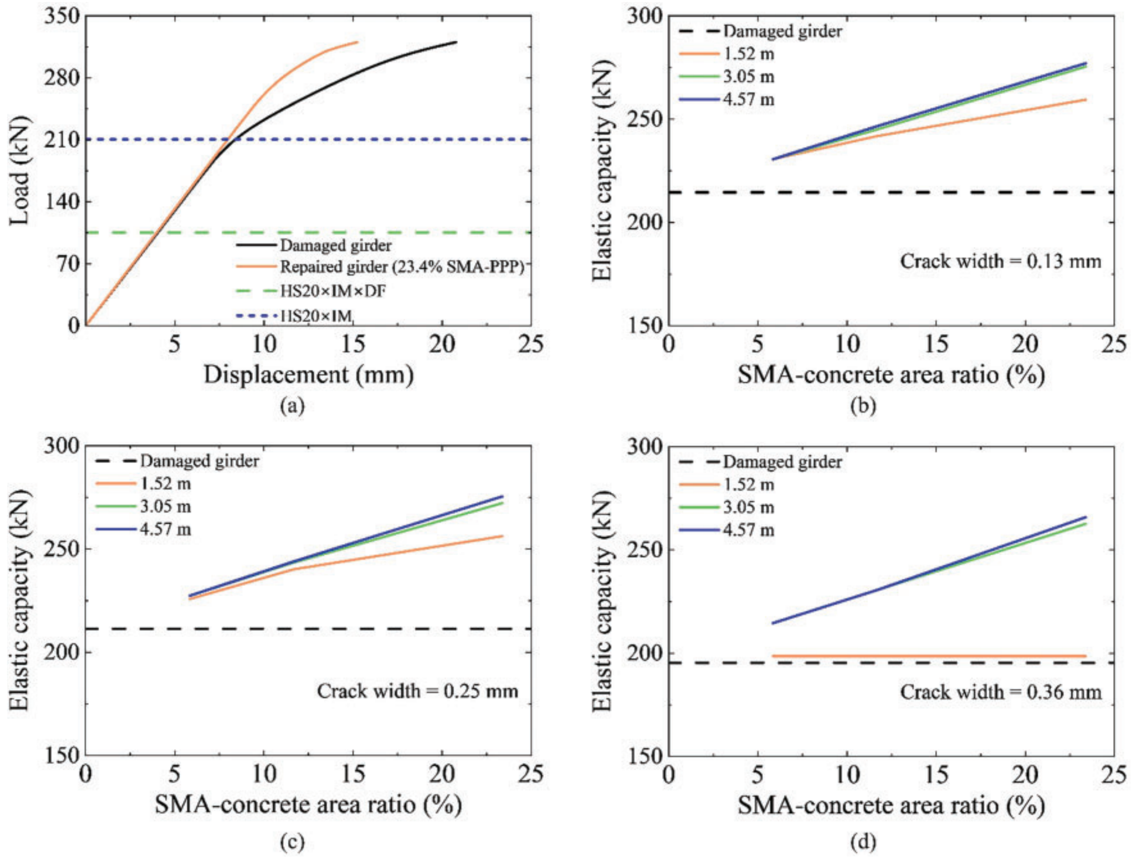

Figure 11. (a) Load–displacement curves of the damaged girder and the girder repaired with a 4.57-m-long 23.4% SMA-PPP, and the elastic capacities of damaged and repaired girders with crack widths of (b) 0.13 mm, (c) 0.25 mm, and (d) 0.36 mm

and 4.57-m-long SMA-PPPs, respectively. The capacity of the repaired girder increased with increasing PPP length up to 3.05 m, after which the rate of increase decreased as the influence of the PPP length on the capacity was reduced. This shows that there is an optimal length for the PPP, beyond which the impact of PPP length on the capacity and global behavior of the repaired girder reduces. For the 13.9-m-long PPC deck girder analyzed in this study, the optimal PPP length was found to be 3.05 m. The initial elastic modulus of the repaired girder increases linearly with increasing PPP length. This behavior was attributed to the increasing influence of the local prestressing effect of the SMA-PPP on the global behavior with increasing PPP length.

As the transverse crack width increases, the elastic capacity of the damaged girder reduces. In Fig. 11, the damaged girder with crack widths of 0.13, 0.25, and 0.36 mm exhibited elastic capacities of 214.6, 211.4, and 195.4 kN, respectively. Upon repairing the damaged girders with a 4.57-m-long 23.4% area ratio SMA-PPP, the elastic capacities improved to 277.04 kN (29.1%), 275.43 kN (30.3%), and 265.9 kN (36.1%), respectively. This shows that repairing damaged girders with SMA-PPPs—from those with hairline (0.13 mm) to larger (0.36 mm) cracks—is highly effective, and the elastic capacity could be improved by up to 36.1%.

In Fig. 11d, the improvement in the elastic capacity of the girder repaired by the 1.52-m-long PPP was only 1.9% for all the SMA–concrete area ratios. In this case, the damaged girder had two transverse cracks, with the larger crack measuring 0.36 mm, compared to the single transverse crack widths of 0.13 and 0.25 mm in the girders considered in Figs. 11b, 11c. The 1.52-m-long PPP was unable to effectively cover both the cracks in the damaged girder due to its shorter length. Thus, the stresses in the repaired crack were redistributed to the crack outside the repair zone, which resulted in the reduced improvement in the elastic capacity of the repaired girders.

Load rating analysis of the repaired girders

In the US, AASHTO MBE provides the standard guidelines and procedures to load rate in-service bridges. It verifies the safety and serviceability of a bridge under the design loads for its current material and structural condition. The load rating of a girder gives the maximum indefinitely allowable live load (given by the inventory rating) and the maximum allowable live load (given by the operating rating) for a bridge.[28] This allows the owner to decide the maximum vehicular load for daily traffic and the occasional overweight vehicular load.

Gunasekaran and Andrawes[27] conducted a parametric study, which observed that the capacity and the strand stresses govern the load rating of a girder damaged by transverse cracks. Therefore, this study closely examined the

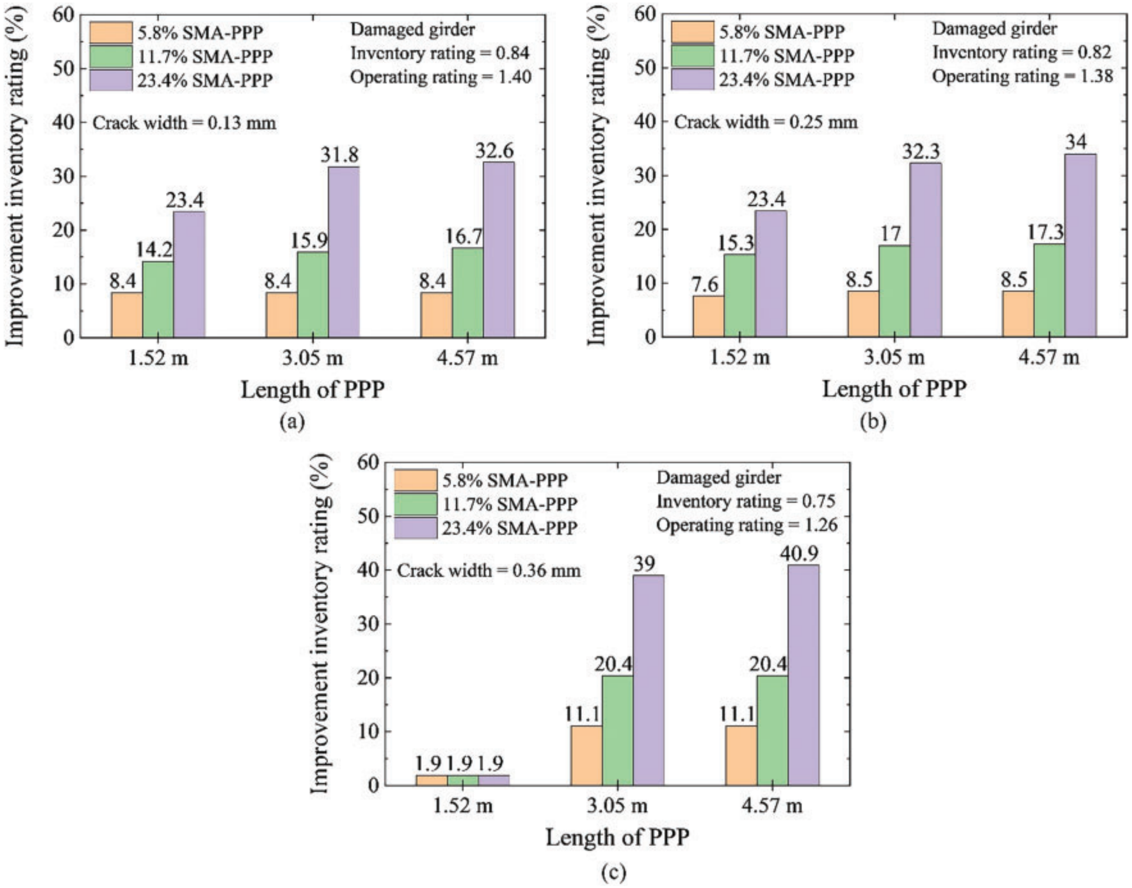

(a)

(b)

(c)

Figure 12. Inventory rating of damaged and repaired girders: (a) hairline cracks (0.13 mm); (b) moderate cracks (0.25 mm); and (c) severe cracks (0.36 mm)

effect of an SMA-PPP on the elastic capacity and the strand stresses of the damaged and repaired girders. The elastic (residual) capacity was used to calculate the capacity-based ratings, while the built-up strand stresses under gravity were used to calculate the rating of the prestressing strands in tension. The load rating of the damaged girder was used as a baseline measure to understand the effect of repairing a girder with SMA-PPP.

The inventory and operating rating equations for the flexural capacity of a girder are given by

$$RF_{Inv\_Strength} = \frac{C - 1.3D}{2.17L\,(1 + I)} \tag{1}$$

$$RF_{Op\_Strength} = \frac{C - 1.3D}{1.3L\,(1 + I)} \tag{2}$$

where C is the nominal moment capacity, D and L are the unfactored dead and live load moments, and I is the IM.

For the 838 mm × 914 mm PPC deck girder considered in the study, the capacity-based load rating governed the inventory and operating ratings of the damaged and repaired girders. Fig. 12 presents the percentage improvement in the inventory and operating ratings[28] of the repaired girders. For the damaged girders with transverse crack widths of 0.13, 0.25, and 0.36 mm, the inventory ratings are 0.84, 0.82, and 0.75, while the operating ratings are 1.40, 1.38, and 1.26, respectively. In Fig. 12a, the inventory rating of the repaired girder increased by 8.4%–32.6% for the 4.57-m-long SMA-PPP. A linear increase in inventory rating with an increase in the SMA area ratio was observed in all cases. The girders repaired with SMA-PPP exhibited a maximum improvement of 40.9% (Fig. 12c) in the capacity-based inventory and operating ratings.

As shown in Fig. 12b, the inventory rating of the repaired girder increased with increasing length of the SMA-PPP. The inventory rating of the repaired girder increased by 23.8%, 32.3%, and 34.0% when repaired with 1.52-, 3.05-, and 4.57-m-long SMA-PPP with an SMA area ratio of 23.4%. The inventory and operating ratings increased with the increasing length of the PPP up to a length of 3.05 m, after which the rate of improvement decreased. This shows that the optimal length of PPP is 3.05 m for the 13.9 m PPC deck girder.

As shown in Fig. 12c, SMA-PPPs were highly effective in repairing damaged girders with a large crack width of 0.36 mm. The inventory rating of the repaired girder increased from 1.9% to 40.9% for the range of PPP lengths and SMA area ratios. The inventory rating of the girder repaired with a 1.52-m-long PPP exhibited minimal improvement as the length of the PPP was not enough to cover all the cracks in the damaged girder.

The girders repaired with a 23.4% area ratio SMA-PPP of all lengths had an inventory rating factor of one or above. This shows that these repaired girders can safely carry an

HS-20 truck. Thus, it was shown that repairing using SMA-PPPs could significantly improve the capacity-based rating values. Girders damaged by transverse cracks could still be used with a suitable repair measure.

Conclusions

This study investigated the feasibility and ease of using larger (6.3 mm diameter) NiTiNb bars as the prestressing component of an external prestressing system (SMA-PPPs) through experimental and numerical analysis. The 6.3-mm NiTiNb bars were successfully used as part of a voided SMA-PPP to prestress a mortar block. The improvement in the flexural capacity of the block was experimentally tested using a four-point bending test. The feasibility of using voided SMA-PPPs to repair a large-scale, transversely cracked PPC deck girder was numerically assessed using ABAQUS. The damaged girder was retrofitted with SMA-PPPs to externally prestress the section and reduce the built-up stresses. The impact of the PPP length, SMA-concrete area ratio, and the width of the transverse crack on the repaired girder's capacity was studied. Furthermore, the load ratings of the damaged and repaired girders were calculated and compared to understand the effectiveness of the adopted repair method. The following are the major conclusions of this study:

- The voided SMA-PPPs, with the 6.3-mm NiTiNb bars, induced a prestress of 2.0 MPa in the mortar block and 3.12 MPa in the PPP after the NiTiNb bars were activated. The numerical model was able to replicate the experimental behavior, with a 7% and 13% difference in the induced stresses in the PPP and mortar block, respectively.
- The mortar block prestressed using the voided SMA-PPP was experimentally tested under a four-point bending load, and the cracking and maximum capacities of the block were found to be 13.8 and 15.8 kN, respectively. Meanwhile, the control block without SMA cracked and failed at 9.2 kN, which is 50% less than the prestressed mortar block. Furthermore, the developed numerical model was validated against experimental flexural test results. The load–deflection response, peak capacity, and stiffness showed good agreement, confirming the model's capability to capture the structural behavior of the SMA-PPP system. The flexural test demonstrated the ability of voided SMA-PPPs to prestress and improve the load-bearing capacity, stiffness, and ductility of a concrete member.
- The numerical analysis of the girders repaired with voided SMA-PPPs exhibited up to a 36.1% improvement in elastic capacity, which resulted in a 40.9% improvement in the inventory rating of the repaired girders.
- The load rating of the girders repaired with 23.4% SMA-PPPs is above one, which implies that these girders can be used to safely carry the live loads induced by an HS-20 design truck indefinitely.
- The numerical analysis predicts an optimal PPP length (3.05 m for the 13.9-m-long girder), beyond which the rate of improvement in elastic capacity decreases. The results of the numerical analysis demonstrated that girders with hairline (0.13 mm) to large (0.36 mm) cracks could be effectively repaired to achieve a load rating above one.

Statements and Declarations

The authors have no relevant financial or non-financial interests to disclose.

Acknowledgements

The authors gratefully acknowledge the financial support provided by the Transportation Infrastructure Precast Innovation Center (TRANS-IPIC) through the University Transportation Center program of the US Department of Transportation, Office of the Assistant Secretary for Research and Technology (OST-R), under Grant No. 69A3552348333.

References

[1] NBI. *National Bridge Inventory*. Fedral Highway Administration; 2022.

[2] Xiaohong S. Cause analysis of transverse cracks and reinforcement measures for midspan of assembled box girder bridge. *IOP Conference Series: Earth and Environmental Science*; 2019.

[3] Gunasekaran D, Mirdad A, Andrawes B. Capacity and load rating of in-service precast prestressed concrete bridge deck girders with transverse cracks. *J Perform Constr Facil*. 2023;37(2):1237. doi:10.1061/jpcfev.cfeng-4261.

[4] Harajli MH. Strengthening of concrete beams by external prestressing. *PCI J*. 1993, 76–88.

[5] Picard A, Massicotte B, Bastien J. Relative efficiency of external prestressing. *Am Soc Civil Eng (ASCE)*. 1995; 1735–1872.

[6] Zhao H, Andrawes B. Local strengthening and repair of concrete bridge girders using shape memory alloy precast prestressing plate. *J Intell Mater Syst Struct*. 2020;31(11).

[7] Zhu H, Yang Y, Fan W. External prestressing bridge reinforcement technology review. *International Conference on Engineering Technology and Application (ICETA 2015)*. vol. 22, 2015; MATEC Web of Conferences:1–5.

[8] Afefy HM, Sennah K, Cofini A. Retrofitting actual-size precracked precast prestressed concrete double-tee girders using externally bonded CFRP sheets. *J Performance of Constructed Facilities*. 2015;30(2):493. doi:10.1061/(asce)cf.1943-5509.0000763.

[9] Chen J, Wang W, Fang C. Manufacturing, testing and simulation of novel SMA-based variable friction dampers with enhanced deformability. *J Build Eng*. 2022;103513.

[10] Cao S, Ozbulut OE, Shi F, Deng J. An SMA cable-based negative stiffness seismic isolator: development, experimental characterization, and numerical modeling. *J Intell Mater Syst Struct*. 2022;1819–1833.

[11] Schranz B, Michels J, Czaderski C, Motavalli M, Vogel T, Shahverdi M. Strengthening and prestressing of bridge decks with ribbed iron-based shape memory alloy bars. *Eng Struct*. 2021

[12] Suhail R, Amato G, Broderick B, Grimes M, McCrum D. Efficacy of prestressed SMA diagonal loops in seismic retrofitting of non-seismically detailed RC beam-column joints. *Eng Struct*. 2021

[13] Sung M, Andrawes B. Innovative local prestressing system for concrete crossties using shape memory alloys. *Eng Struct*. 2021.

[14] Choi E, Hong H-K, Kim HS, Chung Y-S. Hysteretic behavior of NiTi and NiTiNb SMA wires under recovery or prestressing stress. *J Alloys Compounds*. 2013;577(3):444–447. doi:10.1016/j.jallcom.2012.02.037.

[15] Jung D, Wilcoski J, Andrawes B. Bidirectional shake table testing of RC columns retrofitted and repaired with shape memory alloy spirals. *Eng Struct*. 2018;160:171–185. doi:10.1016/j.engstruct.2017.12.046.

[16] Zhao H, Andrawes B. Mechanical properties of NiTiNb shape memory alloy subjected to a harsh corrosive environment. *J Mater Civil Eng*. 2016;29(3).

[17] Andrawes B, Sung M, Park S. NiTiNb shape memory bars for concrete prestressing applications; 2024. https://ssrn.com/abstract=5048485.

[18] Dassault Systèmes Simulia Corp. *ABAQUS, 2024 Analysis User's Manual*. Providence, RI, USA: Dassault Systèmes Simulia Corp; 2024.

[19] Menegotto M, Pinto PE. *Method of Analysis of Cyclically Loaded RC Plane Frames Including Changes in Geometry and Non-Elastic Behavior of Elements Under Normal Force and Bending*. Lisbon: IABSE Symposium on Resistance and ultimate Deformability of Structures Acted on by Well-Defined Repeated Loads; 1973.

[20] Hognestad E. *A Study on Combined Bending and Axial Load in Reinforced Concrete Members*. IL: Univ. of Illinois at Urbana-Champaign; 1951.

[21] Stocker, Sozen. *Investigation of Prestressed Reinforced Concrete for Highway Bridges: Part VI—Bond Characteristics of Prestressing Strand*. Urbana: University of Illinois, Urbana-Champaign; 1969.

[22] Logan DR. Acceptance criteria for bond quality of strand for pretensioned prestressed concrete applications. *PCI J*. 1997, 52–90.

[23] Peterman RJ. Influence of flexure-shear cracking on strand development length in prestressed concrete members. *PCI J*. 2009;143–161.

[24] Loflin BJ. *Bond and Material Properties of Grade 270 and Grade 300 Prestressing Strands*. Virginia Polytechnic Institute and State University; 2008.

[25] Andrawes BO, Pozolo A, Shin M. *Transfer and Development Length of Prestressing Tendons in Full-Scale AASHTO Prestressed Concrete Girders Using Self-Consolidating Concrete*. Urbana: Illinois Center for Transportation; 2009.

[26] Cousins T, Badeaux M, Moustafa S. Proposed test for determining bond characteristics of prestressing strand. *PCI J*. 1992;66–73.

[27] Gunasekaran D, Andrawes B. Parametric study on transversely cracked precast prestressed concrete bridge deck girders with rectangular voids. *Transportation Research Record*. 2024.

[28] AASHTO. *Manual for Bridge Evaluation*. 3rd ed. Washington, DC: American Association of State Highway and Transportation Officials (AASHTO); 2018.